Supplementary Materials and Methods

Plasmid constructions

The fusion protein (HcB-Syt-II) was designed by connecting the C-terminus of HcB, residues 858-1291, to the N-terminus of rat Syt-II, residues 8-61, by a 15 residue linker (PPTPGSAWSHPQFEK) including a Strep-tag. HcB-Syt-II was cloned into the pQE vector with an N-terminal His_6-tag (Qiagen). Plasmids encoding the HcB (pHcBS, residues 858-1291) and the full-length of BoNT/B (pBoNTBS) as well as plasmids encoding the truncated GST-Syt-I (1-53) and GST-Syt-II (1-61) fusion proteins (pGEXSytI-53C and pGEXSytII-61C) used in this study were described previously [1,2]. Mutations of the HcB and GST-Syt-I and Syt-II were generated by PCR using suitable primers and pHcBS, pGEXSytI-53C and pGEXSytII-61C, respectively, as template DNA. Correspondingly mutated expression plasmids for full-length BoNT/B were generated by swapping DNA fragments between pBoNTBS and mutated pHcBS plasmids. Nucleotide sequences of all mutants were verified by DNA sequencing.

Protein expression and purification

Wild-type and mutated recombinant H_CB and full-length BoNT/B were produced, the latter under biosafety level 2 containment, utilizing the *Escherichia coli* strain M15pREP4 (Qiagen). GST-Syt-I (1-53) and GST-Syt-II (1-61) and their mutation variants were expressed in *Escherichia coli* strain BL21-STAR (DE3) (Invitrogen). For expression of each protein, bacteria were grown at 37 °C and induced with 250 μM of isopropyl-β-D-thiogalactopyranoside (IPTG) when OD_{600} absorption reached 0.8-1.0 in TB medium. The temperature was then reduced to 20 °C and the induction was continued for ~16

hours. Cells were harvested and re-suspended in phosphate-buffered saline (PBS) buffer with 0.5 mM PMSF and complete (EDTA free) protease inhibitor cocktail (Roche), and lysed by sonication. For purification of HcB-Syt-II, the clarified cell lysate was first loaded to a Ni-NTA column (Qiagen). After extensive wash with a buffer containing 50 mM sodium phosphate, pH 8.0, 300 mM NaCl, the column was washed with the same buffer supplemented with 10 mM imidazole, and then eluted in the same buffer with 100 mM imidazole. The pooled elution fractions from the Ni-NTA column were then loaded to a 4 ml StepTactin column (IBA) by two passes. The StrepTactin column was washed twice with 10 ml of 100 mM Tris-HCl, pH 8.0 buffer, and the bound protein was eluted with 4.8 ml of 10 mM desthiobiotin in 100 mM Tris-HCl, pH 8.0. HcB-Syt-II was further purified by a HiLoad-16/60 Superdex-200 (GE Healthcare) size exclusion column in a buffer composed of 20 mM Tris-HCl, pH 7.5, 50 mM NaCl. The Strep-tag fused HcB and full length BoNT/B and their variants were one-step purified using StrepTactin resin from IBA according to the manufacturer's instructions. For purification of the GST fusion proteins, the cell lysate was first clarified by centrifugation, loaded to a Glutathione-Sepharose 4B column (GE Healthcare), and then washed extensively with a buffer containing 50 mM Tris-HCl, pH 8.0 and 150 mM NaCl. The wild-type and mutated GST-Syt-I and Syt-II were eluted with 20 mM reduced glutathione. Alternatively, the luminal domain of Syt-II was cleaved with thrombin (Hematologic Technology) on the column. The purity of all purified proteins was over 90% when checked by SDS-PAGE. All experiments were carried out at 4 °C.

Crystallization and diffraction data collection

The purified HcB-Syt-II was concentrated to ~7 mg/ml for crystallization. Initial crystallization screens were carried out using high throughput crystallization screen kits from Hampton Research, Emerald Biostructures and Qiagen. The best crystals were grown at 20 °C by vapor diffusion, and each drop contained a 1:1 (v/v) ratio of protein and reservoir solution. The two different reservoir solutions that yielded diffraction qualify single crystals were (1) 13% PEG 6,000 and 0.1 M Hepes, pH 7.0, and (2) 0.8 M sodium citrate, pH 6.5. Long bar-shape crystals (PEG 6,000 condition) or clusters of thin plate-like crystals (sodium citrate condition) grew to full size in about one week. The crystals were cryoprotected in the same mother liquor supplemented with 20% glycerol, and then flash-frozen in liquid nitrogen. The diffraction data sets were collected at 100 K at beam line 9-1, Stanford Linear Accelerator Center (SSRL), or beam line 8-2-2, Advance Light Source (ALS), using an ADSC Q315 CCD detector. All data were processed using HKL2000 (Supplementary Table 1) [3]. The crystals grown in the PEG 6,000 condition belongs to space group $P2_12_12_1$, with unit cell dimensions a = 55.8 Å, b = 97.5 Å, c = 113.6 Å. Diffraction data were collected to d_{min} = 2.15 Å resolution (Supplementary Table 1). The sodium citrate condition yielded crystals in space group $C222_1$, with unit cell parameters a = 135.1 Å, b = 142.1 Å, c = 60.9 Å, which diffracted to 3.2 Å (data not shown). There is one HcB-Syt-II complex in the asymmetric unit in both crystal forms.

Structure determination

The structure of the HcB-Syt-II complex was determined by molecular replacement using Phaser [4] with HcB as the search model (protein data bank code 1Z0H) [5]. Manual model

building was performed with COOT [6] and all the refinements were carried out with the Crystallography & NMR System (CNS) [7]. Progress was monitored with the free R-value using a 5% randomly selected test set [8].

A lower resolution diffraction data set to 2.6 Å was first used to obtain the molecular replacement solution. Refinements were begun with rigid body minimization followed by a slow-cooling simulated annealing protocol at 5,000 K in the absence of any model for the Syt-II peptide in order to prevent model bias in this region of the electron density. At this point, the R_{work} and R_{free} values were 26.1% and 31.6%, respectively, and the Fo-Fc difference electron density map allowed unambiguous assignment of the Syt-II model (Fig. 1a). A high resolution diffraction data set in the same space group to 2.15 Å was collected at this stage. Iterative rounds of positional and individual B-factor refinement were performed in conjunction with manual model building using the high resolution data set until R_{free} converged. The electron density of HcB was excellent and residues from S858 to E1291 are well defined except for a small disordered region (N1152-I1157). The first two Pro residues in the artificial linker are also modeled. Residues E44 to K60 of Syt-II are structured with residues F47 to I58 forming a long α-helix. The occupancies of the side chains of solvent exposed K49, K51, and K60 are set to zero because of the weak electron density. All other Syt-II residues including the linker residues were not visible. The structure of HcB-Syt-II complex in the $C222_1$ space group was determined by molecular replacement using the high resolution structure as a search model. The new crystal form revealed a different packing arrangement but essentially identical structure (data not shown). The final refinement statistics and maps are excellent (Supplementary

Table 1). In the Ramachandran plots, the number of residues in most favored, additional allowed, or generously allowed regions is 346/52/1 for HcB and 14/0/1 for Syt-II, respectively. No residues are in the disallowed regions. Figures were prepared using programs MOLSCRIPT [9], PyMol (http://www.pymol.org), and Raster3D [10]. Sequence alignment was made using ClustalW[11] and ESPript [12].

Isothermal titration calorimetry

The calorimetry titration experiments were carried out on a VP-ITC calorimeter (MicroCal). HcB was used as a titrand in the cell and GST-Syt-II, GST-Syt-I, or Syt-II was used as titrants in syringe at a tenfold higher concentration. Experiments were performed at 10 °C, 15 °C and 20 °C and up to two protein concentrations for titrations between HcB and GST-Syt-II, and all other experiments were performed at 20 °C. The thermodynamic values reported in the text are the average of two experiments using GST-Syt-II and HcB at 20 °C. All experiments were carried out in the same buffer to control for heat of dilution effects, 50 mM Hepes, pH 7.5 and 150 mM NaCl, except that one experiment was carried out for HcB and GST-Syt-II at a lower pH (50 mM sodium citrate, pH 5.7 and 150 mM NaCl). All protein samples were dialyzed extensively against working solution and, prior to the titration, the samples were degassed for ten minutes. Protein concentrations of HcB, GST-Syt-I and GST-Syt-II were determined using Bradford protein assay (Bio-Rad) and the concentration of Syt-II was quantified by amino acid analysis (University of California, Davis). Data were processed with the MicroCal Origin 7.0 software.

GST pull-down assays

All protein samples were dialyzed against Tris/NaCl/Triton-buffer (20 mM Tris-HCl, 150 mM NaCl, 0.5% Triton X-100, pH 7.2). GST-Syt-I, GST-Syt-II and their variants (0.2 nmol each) immobilized to 10 µl of glutathione-sepharose beads were incubated with HcB or its mutants (0.16 nmol each) in the presence of a bovine brain ganglioside mixture (18% GM_1, 55% GD_{1a}, 10% GT_{1b}, and 2% other gangliosides; Calbiochem; 20 µg each) in a total volume of 400 µl Tris/NaCl/Triton-buffer for 90 min at 4 °C. Beads were collected by centrifugation and washed three times each with 35 bed volumes of the same buffer. Washed pellet fractions were boiled in SDS sample buffer and analyzed together with supernatant fractions by SDS-PAGE and Coomassie Blue staining.

Mouse phrenic nerve toxicity assay

The mouse phrenic nerve (MPN) toxicity assay was set up as described by Habermann *et al.* [13]. Electrical stimulation of the phrenic nerve was continuously performed at a frequency of 1 Hz. Isometric contractions were transformed with a force transducer and recorded with the VitroDat Online software (FMI GmbH). The time required to decrease the amplitude to 50% of the starting value (paralytic halftime) was measured. Recombinant single chain BoNT/B (scBoNT/B) was applied in triplicates at final concentrations of 0.1 nM, 0.3 nM, 1 nM and 3.2 nM. A concentration-response-curve could be described by the power function $y = 54.4x^{-0.3}$ ($R^2 = 1.0$). The resulting paralytic halftimes were converted to the corresponding concentrations of wild-type scBoNT/B using the equation mentioned above. The toxicities were finally expressed as a percentage of wild-type toxicity.

Multi-angle laser light scattering

The multi-angle laser light scattering (MALS) experiment was carried out using a DAWN EOS light scattering unit and an Optilab refractive index detector (Wyatt Technology), combined with a Jasco UV detector, UV-975 (Jasco Corp) and a Shimadzu DGU-14A degasser (Shimadzu Corp). The MALS system was coupled to a Shodex Protein KW-803 size exclusion column (Shodex). The signal from monomeric bovine serum albumin was used to normalize the detector response. The protein sample was at approximately 3 mg/ml. The experiment was performed at ambient temperature (~ 20 °C) in a buffer containing 20 mM Tris-HCl, pH 7.5 and 50 mM NaCl. The flow rate was maintained at 0.5 mg/ml. A value of 0.185 ml/g was assumed for the dn/dc value of the proteins. The data analysis was performed using software ASTRA V 5.1.9.1, as per the manufacturer's instructions.

1. Rummel, A., Karnath, T., Henke, T., Bigalke, H. & Binz, T. Synaptotagmins I and II act as nerve cell receptors for botulinum neurotoxin G. *J Biol Chem* **279**, 30865-70 (2004).
2. Rummel, A., Mahrhold, S., Bigalke, H. & Binz, T. The HCC-domain of botulinum neurotoxins A and B exhibits a singular ganglioside binding site displaying serotype specific carbohydrate interaction. *Mol Microbiol* **51**, 631-43 (2004).
3. Otwinowski, Z. & Minor, W. Processing of X-ray diffraction data collected in oscillation mode. *Methods Enzymol* **276** (1997).
4. McCoy, A. J., Grosse-Kunstleve, R. W., Storoni, L. C. & Read, R. J. Likelihood-enhanced fast translation functions. *Acta Crystallogr D Biol Crystallogr* **61**, 458-64 (2005).
5. Jayaraman, S., Eswaramoorthy, S., Ahmed, S. A., Smith, L. A. & Swaminathan, S. N-terminal helix reorients in recombinant C-fragment of Clostridium botulinum type B. *Biochem Biophys Res Commun* **330**, 97-103 (2005).

6. Emsley, P. & Cowtan, K. Coot: model-building tools for molecular graphics. *Acta Crystallogr D Biol Crystallogr* **60**, 2126-32 (2004).
7. Brunger, A. T. et al. Crystallography & NMR system: A new software suite for macromolecular structure determination. *Acta Crystallogr D Biol Crystallogr* **54**, 905-21 (1998).
8. Brunger, A. T. Free R value: a novel statistical quantity for assessing the accuracy of crystal structures. *Nature* **355**, 472-475 (1992).
9. Kraulis, P. J. MOLSCRIPT: a program to produce both detailed and schematic plots of protein structures. *J Appl Cryst* **24**, 946-950 (1991).
10. Merritt, E. A. & Murphy, M. E. P. Raster3D Version 2.0. A program for photorealistic molecular graphics. *Acta Crystallogr D* **D50**, 869-873 (1994).
11. Thompson, J. D., Higgins, D. G. & Gibson, T. J. CLUSTAL W: improving the sensitivity of progressive multiple sequence alignment through sequence weighting, position-specific gap penalties and weight matrix choice. *Nucleic Acids Res* **22**, 4673-80 (1994).
12. Gouet, P., Robert, X. & Courcelle, E. ESPript/ENDscript: Extracting and rendering sequence and 3D information from atomic structures of proteins. *Nucleic Acids Res* **31**, 3320-3 (2003).
13. Habermann, E., Dreyer, F. & Bigalke, H. Tetanus toxin blocks the neuromuscular transmission in vitro like botulinum A toxin. *Naunyn Schmiedebergs Arch Pharmacol* **311**, 33-40 (1980).
14. Dolinsky, T. J., Nielsen, J. E., McCammon, J. A. & Baker, N. A. PDB2PQR: an automated pipeline for the setup of Poisson-Boltzmann electrostatics calculations. *Nucleic Acids Res* **32**, W665-7 (2004).
15. Baker, N. A., Sept, D., Joseph, S., Holst, M. J. & McCammon, J. A. Electrostatics of nanosystems: application to microtubules and the ribosome. *Proc Natl Acad Sci U S A* **98**, 10037-41 (2001).

Supplementary Table 1 Data collection and refinement statistics

	HcB-Syt-II
Data Collection	
Space group	$P2_1\ 2_1\ 2_1$
Cell dimensions	
a, b, c (Å)	55.8, 97.5, 113.6
α, β, γ (º)	90, 90, 90
Resolution (Å) [a]	2.15 (2.23)
R_{merge} [b]	7.6 (50.7)
$I/\sigma I$ [b]	12.9 (3.0)
Completeness (%) [b]	99.5 (96.1)
Redundancy	7.0
Refinement	
Resolution (Å)	40 – 2.15
No. reflections	32,377
$R_{work/}$ R_{free} (%)	19.9/24.5
No. atoms	
HcB	3,663
Syt-II	149
Water	129
B-factors	
HcB	43.0
Syt-II	65.6
Water	37.8
R.m.s deviations	
Bond lengths (Å)	0.009
Bond angles (º)	1.42

[a] Number in parentheses represents the highest resolution bin.
[b] Values in parentheses are statistics for the last shell of the diffraction data

Supplementary Table 2 Thermodynamic parameters for the binding between HcB and Syt-II [a, b]

complex	T (K)	K_a x 10^7 (M^{-1})	ΔH (kcal mol^{-1})	ΔG (kcal mol^{-1})	ΔS (cal $mol^{-1}K^{-1}$)	N
HcB/GST-Syt-II	283	4.21±0.64	-3.5±0.02	-9.9	22.6	1.1
HcB/GST-Syt-II	283	1.35±0.21	-4.7±0.07	-9.2	15.9	1.0
HcB/GST-Syt-II	288	2.12±0.45	-5.8±0.08	-9.7	13.4	0.9
HcB/GST-Syt-II	293	2.64±0.24	-6.9±0.03	-9.9	10.4	1.1
HcB/GST-Syt-II	293	3.17±0.58	-7.8±0.12	-10.1	7.6	0.9
HcB/Syt-II	293	2.44±0.32	-6.7±0.07	-9.9	11.0	1.1
HcB/Syt-II	293	1.55±0.19	-6.9±0.08	-9.6	9.5	1.1
HcB/GST-Syt-II [c]	293	3.13±0.51	-6.0±0.08	-10.0	13.7	1.0

[a] For two experiments at the same temperature, different protein concentrations were used.

[b] Data were fitted to a single-site model to obtain K_a, ΔH, ΔS and N.

[c] The titration was carried out at pH 5.7, while all the other experiments were performed at pH 7.5

Supplementary Figure 1 Covalently linked Syt-II forms a *cis*-complex with BoNT/B and the linker does not constrain the BoNT/B-Syt-II interactions. **a,** Domain architectures of BoNT/B, Syt-II, and of the HcB-Syt-II fusion construct. **b,** Measurement of molecular mass of the HcB-Syt-II fusion protein by MALS. HcB-Syt-II is mono-disperse and monomeric in solution indicating that the covalently linked Syt-II forms a *cis*-complex with HcB (measured MW ~ 62.2 ± 0.2 kDa). **c,** When Syt-II was linked to full length BoNT/B in the same manner, the toxic activity of the fusion protein was reduced to about 6% residual activity. **d,** The GST-Syt-II can no longer pull-down a fusion protein of BoNT/B and Syt-II. The data in panels (**c-d**) suggest that the Syt-II binding site on BoNT/B or HcB is occupied in the fusion protein.

Supplementary Figure 2 Schematic representation of the BoNT/B-Syt-II interface. The hydrophobic interactions and salt bridges are shown as blue or orange dotted lines, respectively, between the interacting groups.

Supplementary Figure 3 HcB interacts with Syt-II with high affinity. **a,** Titration of Syt-II (1-61) into HcB by ITC at 20 °C and pH 7.5. **b,** Titration of GST-Syt-II (1-61) into HcB by ITC at 20 °C and pH 5.7.

Supplementary Figure 4 Sequence alignment of all seven serotypes of BoNTs. The alignment was carried out with the entire sequence. For simplicity only the regions around the receptor binding site are shown. The secondary structure of

HcB is shown on top and BoNT/B residues that directly interact with Syt-II are highlighted with red dots. The alignment was generated using ClustalW [11] and ESPript [12].

Supplementary Figure 5 The simultaneous binding with membrane-anchored Syt-II and ganglioside imposes geometric restrictions on how BoNT/B binds to the membrane surface. **a-b,** A proposed binding mode of BoNT/B in two views related by 180 degrees. The structure of a sialyllactose bound BoNT/B (PDB code: 1F31) was superimposed with the complex of HcB-Syt-II using the coordinates of the Hc fragment for the alignment. The molecular surface of BoNT/B is shown and colored according to its electrostatic potential. Potential values were calculated with the Amber force field using program PDB2PQR [14] and APBS [15] and shown in the range of -10 K_BT to +10 K_BT. Please note that the two surfaces shown are mostly negatively charged. The figures were created using Pymol (http://www.pymol.org).

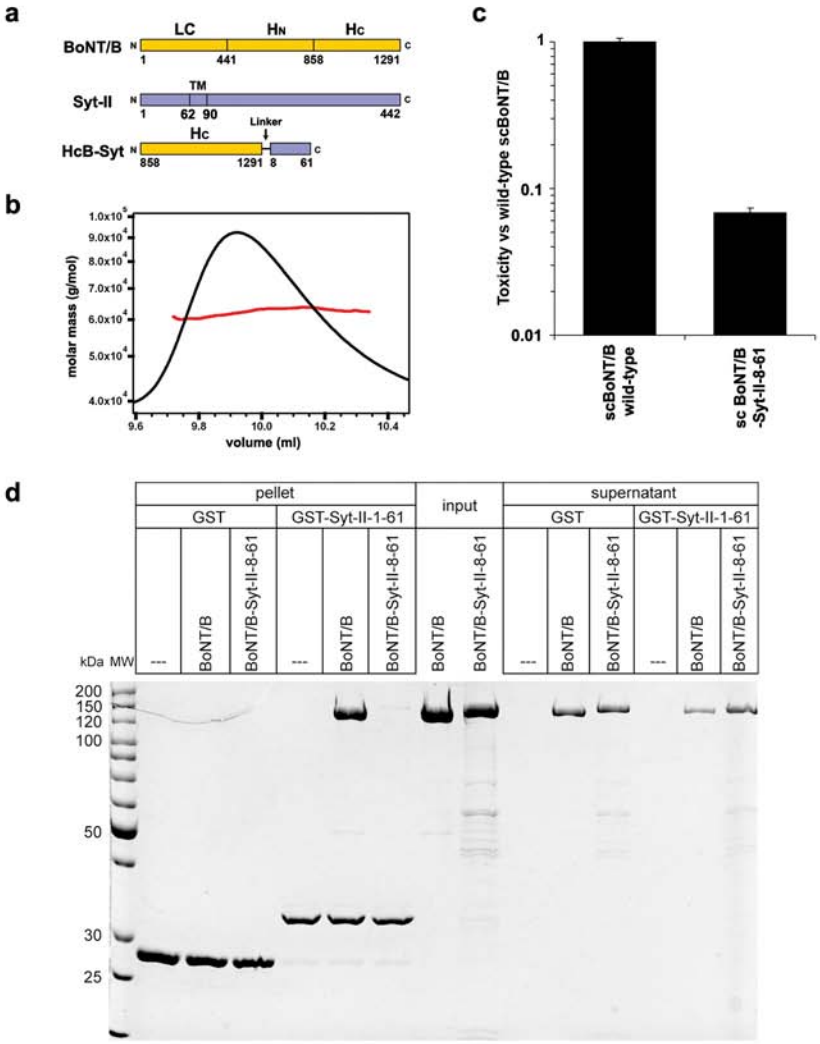

brunger_supplementary_figure1

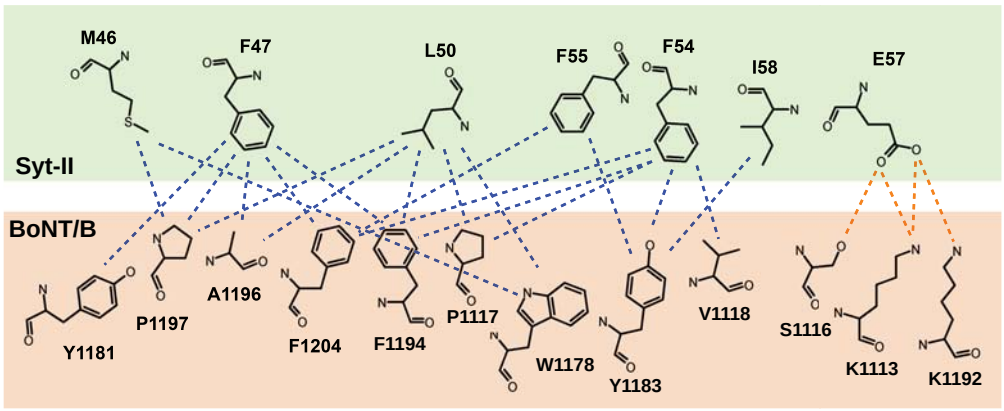

brunger_supplementary_figure2

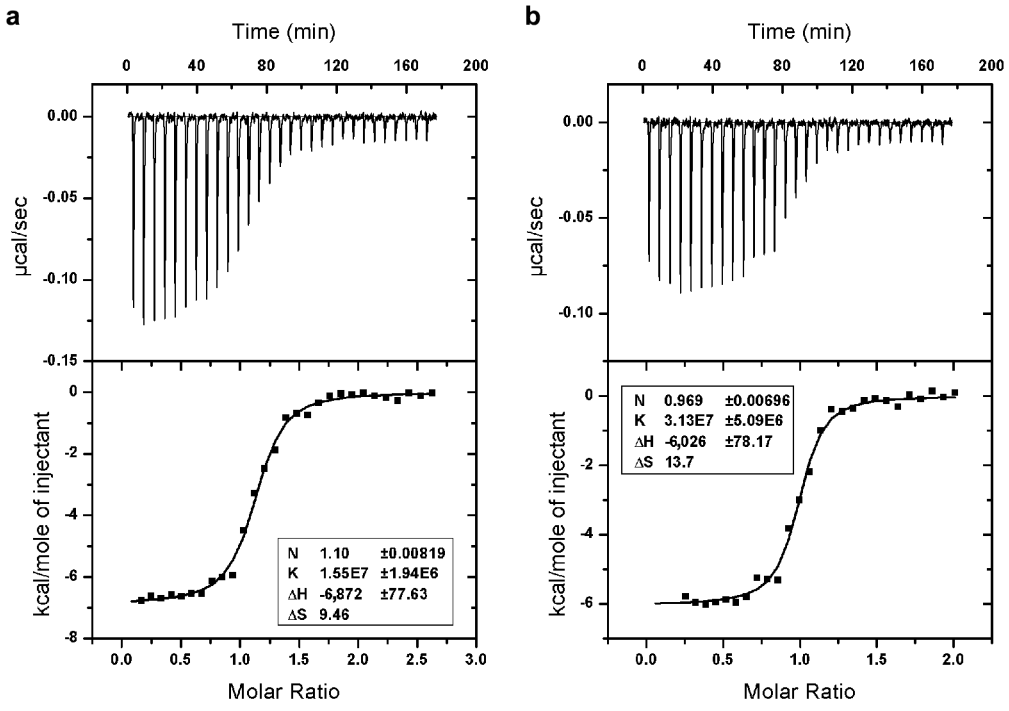

brunger_supplementary_figure3

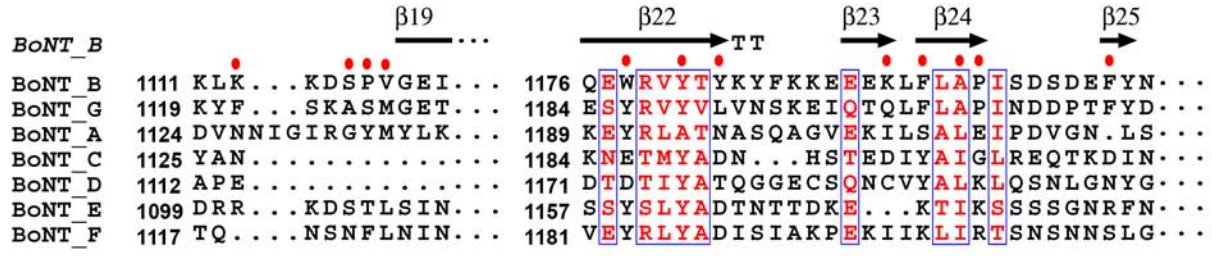

brunger_supplementary_figure4

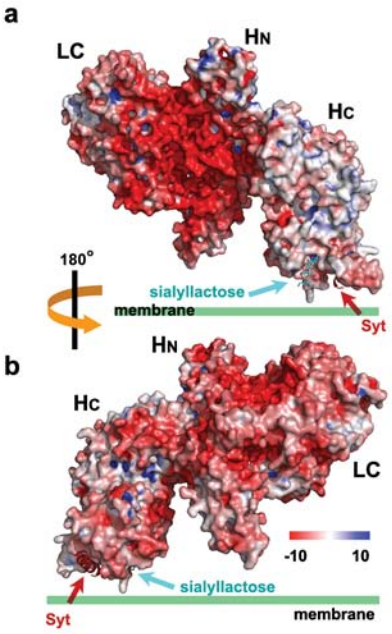

brunger_supplementary_figure5